



HAL
open science

TOPAS-nBio validation for simulating water radiolysis and DNA damage under low-LET irradiation

J Ramos-Méndez, J Laverne, N Domínguez-Kondo, J Milligan, V Štěpán, K Stefanová, Y Perrot, C Villagrasa, W-G Shin, S Incerti, et al.

► To cite this version:

J Ramos-Méndez, J Laverne, N Domínguez-Kondo, J Milligan, V Štěpán, et al.. TOPAS-nBio validation for simulating water radiolysis and DNA damage under low-LET irradiation. *Physics in Medicine and Biology*, 2021, 66 (17), pp.175026. 10.1088/1361-6560/ac1f39 . hal-03334498

HAL Id: hal-03334498

<https://hal.science/hal-03334498>

Submitted on 3 Sep 2021

HAL is a multi-disciplinary open access archive for the deposit and dissemination of scientific research documents, whether they are published or not. The documents may come from teaching and research institutions in France or abroad, or from public or private research centers.

L'archive ouverte pluridisciplinaire **HAL**, est destinée au dépôt et à la diffusion de documents scientifiques de niveau recherche, publiés ou non, émanant des établissements d'enseignement et de recherche français ou étrangers, des laboratoires publics ou privés.



Distributed under a Creative Commons Attribution - NonCommercial - NoDerivatives 4.0 International License

TOPAS-nBio validation for simulating water radiolysis and DNA damage under Low-LET irradiation.

Ramos-Méndez J^{1*}, LaVerne JA², Domínguez-Kondo N³, Milligan J⁴, Štěpán V⁵, Stefanová K⁵, Perrot Y⁶, Villagrasa C⁶, Shin W-G⁷, Incerti S⁸, McNamara A⁹, Paganetti H⁹, Perl J¹⁰, Schuemann J⁹, and Faddegon B¹.

¹ Department of Radiation Oncology, University of California San Francisco, San Francisco, CA 94115, USA.

² Radiation Laboratory and Department of Physics, University of Notre Dame, Notre Dame, IN 46556, USA.

³ Facultad de Ciencias Físico Matemáticas, Benemérita Universidad Autónoma de Puebla, Puebla 72000, MEX.

⁴ Department of Basic Sciences, School of Medicine, Loma Linda University, Loma Linda, CA, 92350, USA.

⁵ Department of Radiation Dosimetry, Nuclear Physics Institute of the Czech Academy of Sciences, Prague, Czech Republic.

⁶ Laboratoire de Dosimétrie des Rayonnements Ionisants, Institut de Radioprotection et Sûreté Nucléaire, Fontenay aux Roses, BP. 17, 92262, France

⁷ Department of Radiation Oncology, Seoul National University Hospital, Seoul 03080, Republic of Korea.

⁸ Univ. Bordeaux, CNRS, CENBG, UMR 5797, F-33170 Gradignan, France

⁹ Department of Radiation Oncology, Physics Division, Massachusetts General Hospital & Harvard Medical School, Boston, MA, USA.

¹⁰ SLAC National Accelerator Laboratory, Menlo Park, CA, USA.

*Corresponding author. Jose.RamosMendez@ucsf.edu

Abstract.

The chemical stage of the Monte Carlo track-structure simulation code Geant4-DNA has been revised and validated. The root-mean-square (RMS) empirical parameter that dictates the displacement of water molecules after an ionization and excitation event in Geant4-DNA has been shortened to better fit experimental data. The pre-defined dissociation channels and branching ratios were not modified, but the reaction rate coefficients for simulating the chemical stage of water radiolysis were updated. The evaluation of Geant4-DNA was accomplished with TOPAS-nBio. For that, we compared predicted time-dependent G values in pure liquid water for $\cdot\text{OH}$, e_{aq}^- , and H_2 with published experimental data. For H_2O_2 and $\text{H}\cdot$, simulation of added scavengers at different concentrations resulted in better agreement with measurements.

In addition, DNA geometry information was integrated with chemistry simulation in TOPAS-nBio to realize reactions between radiolytic chemical species and DNA. This was used in the estimation of the yield of single-strand breaks (SSB) induced by ^{137}Cs γ -ray radiolysis of supercoiled pUC18 plasmids dissolved in aerated solutions containing DMSO. The efficiency of SSB induction by reaction between radiolytic species and DNA used in the simulation was chosen to provide the best agreement with published measurements.

An RMS displacement of 1.24 nm provided agreement with measured data within experimental uncertainties for time-dependent G values and under the presence of scavengers. SSB efficiencies of 24% and 0.5% for $\cdot\text{OH}$ and $\text{H}\cdot$, respectively, led to an overall agreement of TOPAS-nBio results within experimental uncertainties. The efficiencies obtained agreed with values obtained with published non-homogeneous kinetic model and step-by-step Monte Carlo

1
2
3 simulations but disagreed by 12% with published direct measurements. Improvement of the
4 spatial resolution of the DNA damage model might mitigate such disagreement.

5
6 In conclusion, with these improvements, Geant4-DNA/TOPAS-nBio provides a fast,
7 accurate, and user-friendly tool for simulating DNA damage under low LET irradiation.
8
9

10 1 Introduction.

11 A reliable way to study the underlying channels of radiobiological damage is mechanistic
12 modeling. The modeling task is accomplished with Monte Carlo track-structure (MCTS) codes that
13 have the capability of combining complex DNA geometry models with the stochastic processes
14 of the interaction of ionizing radiation with matter and the subsequent non-homogeneous
15 chemistry processes to produce initial DNA damage. MCTS codes specific for radiobiological
16 applications include KURBUC (Nikjoo *et al* 2016), PARTRAC (Dingfelder *et al* 1999), Geant4-DNA
17 (Incerti *et al* 2010a, 2010b, Bernal *et al* 2015), RITRACKS (Plante and Devroye 2017), RADAMOL
18 (Štěpán and Davidková 2014), and TOPAS-nBio (Schuemann *et al* 2018). The reported results
19 obtained with such codes demonstrate the usability of the Monte Carlo method to quantify DNA
20 damage-induced at early stages following irradiation from first principles.
21
22

23 MCTS codes, being flexible mechanistic tools initially developed for liquid water
24 calculations, have demonstrated acceptable accuracy in estimating DNA damage induced by
25 ionizing radiation from first principles. However, many radiobiology-oriented MCTS codes
26 overestimate the yields of $\cdot\text{OH}$ radical produced by fast electrons in liquid water within the
27 nanosecond time scale (Kreipl *et al* 2009, Uehara and Nikjoo 2006, Ramos-Méndez *et al* 2018,
28 Boscolo *et al* 2018). This inaccuracy might potentially mislead the interpretation of calculated
29 DNA damage yields and hence requires benchmarking. In this work, we aim to reconcile MCTS by
30 comparing simulated with experimentally measured yields from the literature for radiolytic
31 species produced by fast electrons at the earliest times.
32
33

34 Experimental validation is paramount to determine the accuracy of the Monte Carlo
35 method. A common approach among MCTS codes assumes that, from the physics perspective,
36 liquid water is sufficient to represent biological tissue (Friedland *et al* 2017, Nikjoo *et al* 2016,
37 Sakata *et al* 2019, Zhu *et al* 2020b). For this reason, MCTS validation relies upon the comparison
38 between calculated quantities with measurements performed in gas or liquid water (see e.g.,
39 (Burigo *et al* 2016, Kreipl *et al* 2009, Pimblott and LaVerne 1997)). Under low linear energy
40 transfer (LET) irradiation, e.g., 0.4 keV/ μm track-averaged LET for ^{137}Cs (Bruce *et al* 1963), the
41 highest contribution to DNA lethal damage is caused by reactions with hydroxyl radicals produced
42 in the radiolysis of water (e.g. > 70% for ^{60}Co , estimated with DNA plasmids pBR322 at scavenging
43 capacities below $\sim 5 \times 10^8 \text{ s}^{-1}$) (Klimczak *et al* 1993). Therefore, thorough validation of the models
44 used by MCTS to simulate the chemical stage in the radiolysis in water is crucial. This task has
45 been accomplished typically by comparing calculated time-dependent yields in pure liquid water
46 with measurements performed in solutes at different scavenging capacities. Subsequently, MCTS
47 codes have been tuned to match the experimental yields at the earliest times available to date.
48
49

50 The accuracy of experimental measurements of radiolytic yields continuously improves.
51 Nowadays, the most accurate picosecond-level measurements of radiolytic yields produced in
52 liquid water by fast electrons have been performed with electron pulse radiolysis. The most
53 recent measurements have determined reference G values (number of chemical species created
54
55
56
57
58
59
60

1
2
3 or lost per 100 eV of energy deposit) for hydroxyl radicals ($\cdot\text{OH}$) of 4.8 ± 0.2 molec./100 eV and
4 solvated electron (e^-_{aq}) yields of 4.2 ± 0.2 molec./100 eV after just 7 ps (El Omar *et al* 2011) (Wang
5 *et al* 2018). These values are significantly lower than previous values used to calibrate Monte
6 Carlo simulations (see e.g., (Tomita *et al* 1997, Kreipl *et al* 2009, Pimblott *et al* 1996, Uehara and
7 Nikjoo 2006) and call for revisiting the input parameters of MCTS codes. A re-evaluation of such
8 parameters has been mentioned for the radiation chemistry code IONLYS-IRT (Sanguanmith *et al*
9 2013, Sultana *et al* 2020); however, specific details of parameter adjustment were not reported.

10
11
12 On the other hand, to verify the accuracy of MCTS for radiobiology applications,
13 sophisticated DNA models have been developed based on the whole cellular nucleus to identify
14 and quantify clustered DNA strand breaks sites (Nikjoo *et al* 2016, Friedland *et al* 2017, Štěpán
15 and Davidková 2014, Meylan *et al* 2017, Lampe *et al* 2018b, Sakata *et al* 2019, Zhu *et al* 2020a).
16 The spatial resolution of experimental measurements at the cellular level is insufficient to
17 validate Monte Carlo simulation outputs directly; for example, experimental techniques can still
18 not resolve spatial distributions of individual DNA single-strand breaks (SSB) and double-strand
19 breaks (DSB), and there is insufficient data about the structure and the radiation chemistry of
20 chromatin. Thus, different assumptions have been made by different research groups to
21 reconcile their MCTS results with experimental data, which impacts the accuracy of the codes. In
22 particular, the scavenging capacity of the biological environment has been mimicked by limiting
23 the time domain to a few nanoseconds. Moiseenko *et al.* (Moiseenko *et al* 1998) showed that
24 this approach introduces 20%-30% differences in strand break yields compared to the explicit
25 simulation of scavenger molecules uniformly distributed around the radiation spurs. Besides, the
26 simulation of the chemical and biological mechanisms occurring within a cell is not a trivial task
27 (Wardman 2020), and MCTS simulations have not yet utilized the corresponding models to
28 simulate more reliable cellular conditions.

29
30
31
32
33 The selection of a less complex biological system than a cell would assist in providing
34 relevant data to evaluate the accuracy of MCTS. Plasmids of DNA are a convenient example.
35 Experiments consisting of the irradiation of plasmids can be performed in a well-controlled
36 environment with solutes of various scavenging capacities (Milligan *et al* 1996). Thus, under low
37 LET irradiation, direct comparison with plasmid experiments provides a suitable way to validate
38 directly MCTS radiochemistry capabilities. Comparison of MCTS with plasmid experiments
39 considering direct and indirect damages has been performed in the past (Tomita *et al* 1998)
40 (Fulford *et al* 2001) (Edel *et al* 2006).

41
42 In this work, we focus on the comparison of calculated versus published measured data
43 to evaluate the accuracy of TOPAS-nBio. Parameters for modeling the radiation chemistry
44 process of TOPAS-nBio were revisited, driven by the latest published experimental
45 measurements of G values of radiation yield for fast electrons at the picosecond level. In that
46 way, a reconciliation between measured and Monte Carlo modeled G values in liquid water was
47 achieved. Then, we validated TOPAS-nBio for simulation of indirect damage of DNA. To this end,
48 experimental setups of plasmids under low-LET irradiation reported in the literature were
49 replicated with our validated Monte Carlo track-structure tool. Our benchmarked code provides
50 a tool over which extended features regarding effects of temperature, compaction of DNA,
51 oxygen concentration and other radiation chemistry processes may be implemented and
52 evaluated.
53
54
55
56
57
58
59
60

2 Materials and methods.

The physics list comprises models describing the discrete transport of electrons in liquid water with no production cuts for secondary electrons, and all the interaction events are explicitly simulated. The selected models have been described extensively elsewhere (Incerti *et al* 2018, Shin *et al* 2019, Ramos-Méndez *et al* 2020). In brief, the physics list, encapsulated in the “G4EmDNAPhysics_option2” constructor, includes an elastic scattering model based on the partial wave theory and an inelastic scattering model based on the formalism of the complex dielectric response function of liquid water. For the latter model, four ionization shells and five discrete electronic excitation states are considered. In Geant4-DNA, after an ionization has taken place, the energy of the emitted secondary electron is calculated from the differential (in energy transfer) ionization cross section, which is described by the so-called Born ionization model. This model applies to weakly bound electrons in the liquid water molecule and adopts the dielectric response function formalism. In the case of K-shell ionization (of the oxygen atom), the atomic model Binary-encounter-Approximation-with-Exchange (BEAX) is used. Both models are described in more detail in Incerti *et al* (2018) and references therein. Models to simulate vibrational excitation and electron attachment processes are also included in the constructor.

The reaction kinetics is calculated with the independent reaction times method, IRT (Tachiya 1983, Clifford *et al* 1986, Green *et al* 1990, Pimblott *et al* 1991). The implementation in TOPAS-nBio is described elsewhere (Schuemann *et al* 2018, Ramos-Méndez *et al* 2020). The simulation of scavengers is performed with the continuum approximation (Pimblott *et al* 1991) where it is assumed that the scavenging molecules are uniformly distributed in the background. Then, the probability of chemical species potentially reacting with the background at time t is described by an exponential distribution given by $1 - \exp(-k[B] t)$, where the product of reaction rate k and scavenger concentration $[B]$, $k[B]$, is the scavenging capacity of the background. Instantaneous scavenging within reaction distance R , at the time of chemical species creation, is performed with a probability given by $\exp(-4\pi R^3[B]/2)$ (Pimblott *et al* 1991). The reactions and rate constants used in this work are presented in table 1, obtained from (Pimblott 1992). These values originated from the National Institute of Standards and Technology (NIST) database (Buxton *et al* 1988), where each rate constant was evaluated for accuracy and consistency.

2.1 Validation of TOPAS-nBio for water radiolysis simulations for fast electrons.

To validate TOPAS-nBio, we revisit Geant4-DNA (version 10.6.p03) parameters for the simulation of the pre-chemical stage of water radiolysis previously reported (Kreipl *et al* 2009, Karamitros *et al* 2011, Ramos-Méndez *et al* 2018, Shin *et al* 2019). Prior to the dissociation of the ionized water molecules (H_2O^+), hole migration by electron correlation and electron relaxation (charge migration) results in a displacement of these molecules and their dissociation products from the place of energy transfer (Ogura and Hamill 1973, Despré *et al* 2015, Kuleff *et al* 2016). In Geant4-DNA, this process is considered by adding an isotropic displacement from where the ionization event occurred. The distance is sampled from a normal distribution with a given root-mean-square deviation (RMS). Due to the lack of measured data at the pre-chemical stage, the root-mean square (RMS) values (inherited from the PARTRAC code) are set to match measured yields of $\cdot\text{OH}$ radical available in 2009 (Kreipl *et al* 2009). In Table 2, the distances used in Geant4-

DNA are described. In this work, the selection of empirical values $RMS^{H_2O^+}$ and $RMS^{H_2O^*}$ is driven by experimental G values for $\cdot OH$ radicals obtained at the picosecond time range for fast electrons reported in (Wang *et al* 2018). We increased the displacement distance in multiples of the mean separation between water molecules, 0.31 nm (Perkins 1986), to minimize the discrepancy with measured data. The branching ratios are kept unchanged, as reported in table 4 in (Shin *et al* 2019) and originally reported in (Kreipl *et al* 2009).

The thermalization of sub-excited electrons is simulated using a “one-step model” with displacement parameters obtained from the literature. The transport of each individual sub-excited electron is stopped once its kinetic energy is reduced to <10 eV. Later, in this one-step model, a solvated electron is placed at a distance (around the last interaction point) randomly sampled from a Gaussian distribution, with a standard deviation given by the data reported in (Ritchie *et al* 1994), with the correction factor described in (Shin *et al* 2019). The data from Ritchie *et al*, 1994, provided the best agreement with measured data of the time-dependent G-values for solvated electrons from (El Omar *et al* 2011) when using the physics list selected in this work. This model and other approaches to simulate the thermalization of solvated electrons have been discussed in detail elsewhere (Shin *et al* 2019).

Table 1 List of reaction rate constants used for the simulation of G values obtained from (Buxton et al 1988) (Milligan et al 1996) (Pastina and LaVerne 1999) and (Huerta Parajon et al 2008)

Reactions for simulation of radiolysis in pure liquid water.		Reactions with scavengers for DNA damage simulation.	
Reaction	k_{obs} (/M/s)	Reaction	k_{obs} (/M/s)
$e^-_{aq} + e^-_{aq} \rightarrow H_2 + OH^-$	5.5×10^9	$e^-_{aq} + O_2 \rightarrow O_2^-$	1.9×10^{10}
$e^-_{aq} + H_3O^+ \rightarrow H\cdot$	2.3×10^{10}	$H\cdot + O_2 \rightarrow HO_2$	2.1×10^{10}
$e^-_{aq} + H\cdot \rightarrow H_2 + OH^-$	2.5×10^{10}	$\cdot OH + DMSO$	7.1×10^9
$e^-_{aq} + \cdot OH \rightarrow OH^-$	3.0×10^{10}	$H\cdot + DMSO$	2.7×10^6
$e^-_{aq} + H_2O_2 \rightarrow OH^- + \cdot OH$	1.1×10^{10}	$e^-_{aq} + DMSO$	3.8×10^6
$H_3O^+ + OH^- \rightarrow H_2O$	14.3×10^{10}		
$H\cdot + H\cdot \rightarrow H_2$	7.8×10^9		
$H\cdot + \cdot OH \rightarrow H_2O$	1.55×10^{10}		
$H\cdot + H_2O_2 \rightarrow \cdot OH + H_2O$	9.0×10^7		
$\cdot OH + \cdot OH \rightarrow H_2O_2$	5.5×10^9		
		Reactions for calculating G(H₂O₂)	
		Reaction	k_{obs} (/M/s)

Reactions with DNA		Reactions for calculating G(H')	
Reaction	k_{obs} (/M/s)	Reaction	k_{obs} (/M/s)
$\cdot\text{OH} + \text{DNA}$	Variable	$\cdot\text{H} + \text{HCO}_2^- \rightarrow \text{H}_2$	2.1×10^8
$\text{H} \cdot + \text{DNA}$	0.03×10^9	$+\cdot\text{CO}_2^-$	
$e_{\text{aq}}^- + \text{DNA}$	0.01×10^9	$e_{\text{aq}}^- + \text{NO}_3^- \rightarrow \text{NO}_3^{2-}$	9.7×10^9
		$\text{Br} + \cdot\text{OH} \rightarrow$	1.1×10^{10}

The simulation setup consists of a homogenous liquid water box (1 g/cm³ density) irradiated with monoenergetic electrons of 1 MeV. This setup is commonly used to simulate MCTS codes for fast electrons, as reported elsewhere (Pimblott and LaVerne 1997, Uehara and Nikjoo 2006, Ramos-Méndez *et al* 2018). Specifically, an isotropic electron source is positioned in the center of a cubic water phantom of 1 cm side. When the primary electron has lost more than 10 keV, the tracking of the electron is stopped, and it is removed from the simulation. The secondary electrons are then followed until their kinetic energy is reduced at or below 10 eV, the low energy limit of the ELSEPA model (Shin *et al* 2018). After that, thermalization is simulated with the one-step model. The total energy deposited in the aqueous medium thus corresponds to the energy lost by the primary electron, which is at least 10 keV (Karamitros 2012). Immediately, the pre-chemical stage takes place, and the initial position of radiolytic products are obtained and input to the IRT method for the simulation of the chemical stage up to 10 μs .

Table 2 Displacements of physical and dissociation products implemented in Geant4-DNA.

Physical product	Dissociation products	$RMS^{H_2O^+}$ or $RMS^{H_2O^*}$	Displacement	
H_2O^+	$\text{H}_3\text{O}^+ + \cdot\text{OH}$ ⁽¹⁾	2.0 nm	H_3O^+	0 or 0.8 nm ⁽²⁾
			$\cdot\text{OH}$	0.8 or 0 nm ⁽²⁾
H_2O^*	$\text{H} \cdot + \cdot\text{OH}$	2.4 nm	$\text{H} \cdot$	$17/18 RMS^{H_2O^*}$
			$\cdot\text{OH}$	$1/18 RMS^{H_2O^*}$
	$\text{H}_2 + 2 \cdot\text{OH}$	0.8 nm	H_2	$2/18 RMS^{H_2O^*}$
			$\cdot\text{OH}$	$16/18 RMS^{H_2O^*} + 0.55 \text{ nm}$
			$\cdot\text{OH}$	$16/18 RMS^{H_2O^*} + 0.55 \text{ nm}$ ⁽³⁾
	$\text{H}_2 + \cdot\text{OH} + \text{OH}^-$	0.8 nm	H_2	$2/18 RMS^{H_2O^*}$

			•OH OH ⁻	16/18 $RMS^{H_2O^*} + 0.55$ nm 16/18 $RMS^{H_2O^*} + 0.55$ nm ⁽³⁾
<p>(¹) If e⁻_{aq} are produced after an autoionization event, then its position is sampled using the one-step thermalization model. See the text.</p> <p>(²) Either value is selected randomly with 50% probability.</p> <p>(³) Positioned in the opposite direction from the first •OH</p>				

A comparison with reference data for H₂, H[•], and H₂O₂ was performed. For H₂, data was obtained from (Pastina *et al* 1999). The authors stated that reported G values are suitable for direct comparison with Monte Carlo simulations without scavengers. For H₂O₂ and H[•], the scavenger system used in the experiments was replicated in our simulations. G values of H₂O₂ measured in solutions containing NO₃⁻ at a concentration of 25 mM, and CH₃OH at concentrations ranging from 10⁻³ – 10 M, were obtained from (Hiroki *et al* 2002). For H[•], measured G values in solutions containing 1 mM of Br, 1 mM of NO₃⁻ and HCO₂⁻ at a concentration ranging from 10⁻² – 1 M were obtained from (Huerta Parajon *et al* 2008). For the latter set of data, replicating the experiment, the calculated yield of H[•] was estimated from the total yield of H₂ calculated with HCO₂⁻ subtracted from the total yield of H₂ calculated without HCO₂⁻ (Huerta Parajón 2010). The reactions used for simulations in the presence of scavengers are shown in table 1. The irradiation setup was the same as that used for pure liquid water simulations.

2.2 Validation of TOPAS-nBio for damage in supercoiled DNA plasmid.

The validation of DNA damage under low-LET irradiation was performed for the experimental conditions from plasmid DNA in aerobic aqueous solution irradiated with ¹³⁷Cs γ-rays, as reported in (Milligan *et al* 1993, Milligan and Ward 1994). A two-stage simulation was performed using condensed-history and track-structure Monte Carlo with TOPAS and TOPAS-nBio, respectively, as described below.

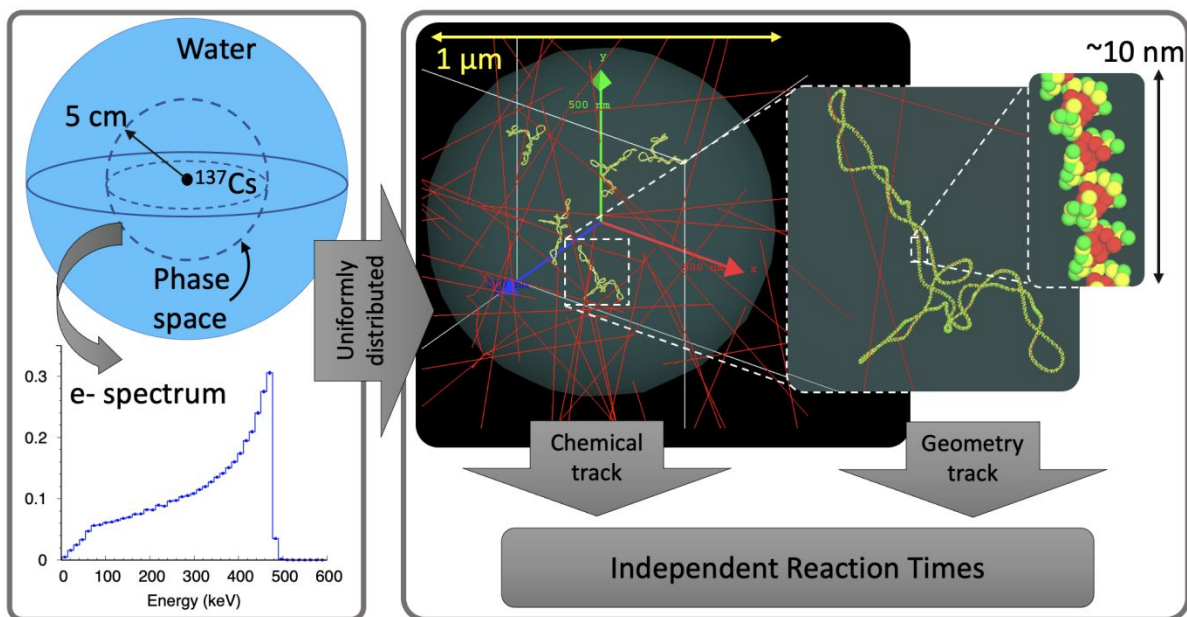
The first stage was used to determine the energy spectrum, at electronic equilibrium conditions, of secondary electrons set in motion by ¹³⁷Cs γ-rays interacting in a water phantom. For that, the TOPAS tool (Perl *et al* 2012, Faddegon *et al* 2020) version 3.5 was used to simulate a concentric system of two homogenous spherical water phantoms of 5 cm and 10 cm radius, respectively. The physics list used the constructor “G4EmStandardPhysics_option4” with a production cut for secondary electrons of 0.05 mm, extensively benchmarked for applications in medical physics (Arce *et al* 2021). An isotropic point source of monoenergetic γ-rays (662 keV) was positioned at the center, as shown in figure 1. We obtained the vertex kinetic energy spectrum (at the position of creation) of those secondary electrons that reached a phase space tallied on the surface of a 5 cm radius sphere. In total, 4 x 10⁸ γ-rays were simulated.

The second stage consists of track-structure Monte Carlo simulations with TOPAS-nBio. The following assumptions are made for simulating the interactions of secondary electrons and reactions of chemical species with DNA molecules. All the medium, including the region occupied by the DNA geometry is made of liquid water. For biological targets, a canonical double helix B-DNA configuration is considered. The DNA sugar-phosphate groups and nucleobases, represented as cut spheres in figure 1, are the main target of the radiation or chemical species

1
2
3 to cause DNA damage. The spatial coordinates of the centroids of the semi-spheres
4 corresponding to sugar-phosphate groups are included in the IRT method for the realization of
5 reactions with the chemical species produced in the water radiolysis process. The coordinates
6 are determined by the supercoiled path, which defines the plasmid DNA model (see below). DNA
7 nucleobases are not included in the reaction kinetics because observed rate constants between
8 chemical species and DNA are used (Tomita *et al* 1998, Perry *et al* 2020), but they are present for
9 ionization/excitation interactions (see below). For the simulated time domain of the chemical
10 stage (10^{-12} – 10^{-4} s), the plasmid DNA model is assumed static. Accumulation of energy deposition
11 of at least 17.5 eV in the sugar-phosphate volumes is considered to register an SSB from direct
12 physical interactions (see (Lampe *et al* 2018a, Zhu *et al* 2020b) and references therein). Chemical
13 species originated from radiolysis occurring within the regions occupied by the DNA semi-spheres
14 are not included in the reaction kinetics and are eliminated upon creation, i.e., no DNA radiolysis
15 is simulated.
16
17
18

19 For modeling indirect damage, a SSB is registered with specific efficiency after the
20 reaction between $\bullet\text{OH}$ and DNA (as a whole) occurred (Önal *et al* 1988, Milligan *et al* 1993,
21 Klimczak *et al* 1993). The reaction rate coefficient for the $\bullet\text{OH}+\text{DNA}$ reaction (table 1) depends
22 on the scavenging capacity of the irradiated environment and is obtained from measured data
23 reported elsewhere (Milligan *et al* 1996). For H^\bullet and e^-_{aq} , constant reaction rates are used as
24 obtained from (Buxton *et al* 1988). We estimate the DNA strand break efficiencies of $\bullet\text{OH}$ and H^\bullet
25 by minimization. We compare calculated to measured data applying a minimization algorithm
26 using the Nelder-Mead method (Nelder and Mead 1965) to find the best efficiency values. For e^-_{aq} ,
27 no strand breaking in DNA is counted as it has not been observed experimentally (Jones and
28 O'Neill 1991), but reactions with DNA are included as e^-_{aq} binds efficiently with nucleobases
29 (Kumar *et al* 2019).
30
31
32

33 The DNA model is wrapped around supercoiled paths to reconstruct pUC18 plasmids
34 (length of 2686 base-pairs length) utilizing DNAfabric (Meylan *et al* 2015). In a separate
35 simulation, the geometric model of the pUC18 plasmid (Yanisch-Perron *et al* 1985) is constructed
36 by the worm-like chain method and subsequent smoothing to base-pair level. First, the
37 supercoiling of a circular plasmid represented by 91 linear segments is modeled using the elastic
38 worm-like chain code developed by the group of A. Vologodskii (Vologodskii and Cozzarelli 1994,
39 Huang *et al* 2001). The temperature is set to 298 K, the superhelical density to -0.06, and the step
40 length to 500 ps. Resulting coarse configurations are converted to sets of 2686 equidistant points
41 along a smooth path using an in-house code implementing the approach of Kümmerle and
42 Pomplun (Kümmerle and Pomplun 2005). One sample supercoiled plasmid configuration is
43 selected for the Monte Carlo simulation of DNA damage.
44
45
46
47
48
49
50
51
52
53
54
55
56
57
58
59
60



Condensed-history Monte Carlo

Track-structure Monte Carlo

Figure 1 Setup showing a two-stage simulation. The condensed-history MC simulation setup used to retrieve the secondary electron spectrum is shown on the left side. The track-structure MC simulation setup used to calculate SSB and DSB yields using supercoiled plasmid DNA is shown on the right side. Red lines correspond to few electron tracks. For more details, see the text.

The plasmid is positioned multiple times inside a spherical water phantom of 0.5 μm radius. The positions and orientations of the plasmids are uniformly random. The sphere is centered in a cubic water box of 2 μm side. A volumetric electron source is uniformly distributed in the cubic box, including the sphere. The initial electron spectrum is calculated in the first stage using a condensed-history Monte Carlo, where the initial directions are set to be isotropic (figure 1). In the experiment (Milligan *et al* 1993), the DNA is dissolved in an aerated solution containing DMSO. Thus, we simulated the scavenging behavior of that solution using the reaction rates shown in Table 1 for e^-_{aq} and H^* with O_2 , using a concentration of 21% O_2 ($0.27 \times 10^{-3} \text{ mol dm}^{-3}$). We report the G value of SSBs using the same units of the experimental data ($\mu\text{mol J}^{-1}$) as a function of scavenging capacity for DMSO. In this way, measured results from (Perry *et al* 2021) performed with different scavenger can be included. The DMSO concentrations range from 0.5×10^{-4} to 1 mol dm^{-3} and the DNA concentration is $50 \mu\text{g mL}^{-1}$. We estimated that nine pUC18 plasmids in the spherical phantom of 0.5 μm radius are equivalent to approximately $50 \mu\text{g mL}^{-1}$ of DNA concentration ($50 \times 10^{-6} \text{ g mL}^{-1} \times 10^3 \text{ L}^{-1} \times \text{mL} / (2686 \text{ bp} \times 650 \text{ g mol}^{-1} \text{ bp}^{-1}) \times N_{\text{av}} \times 5.24 \times 10^{-16} \text{ L} \approx 9$). Results for calculated SSB yields as a function of DNA concentration (from 10 – 200 $\mu\text{g mL}^{-1}$) for a concentration of $10^{-3} \text{ mol dm}^{-3}$ DMSO are also reported. Finally, the yield of SSB and DSB as a function of $\cdot\text{OH}$ scavenging capacity (from 7.1×10^5 – $7.1 \times 10^9 \text{ s}^{-1}$) are reported. A DSB was scored when there was no more than a 10 base-pair distance between at least two SSB's occurring in opposite DNA strands. The total number of simulation jobs with independent random number seeds were 200 to 500, achieving statistical uncertainties from 0.7% to 5% (one standard deviation) for the simulation with the lowest and highest DMSO concentration, respectively. On average, 1150 ± 80 primary histories are generated in each simulation job to

achieve an absorbed dose of 30 Gy in the spherical phantom. In a systematic study (not shown) we found that 30 Gy absorbed dose provided a reasonable computing memory and speed, resulting from the number of primary yields used in the IRT and their processing time. The simulations take between 3 to 6 minutes to complete on a single core of a 2.7 GHz 12-Core Intel Xeon E4.

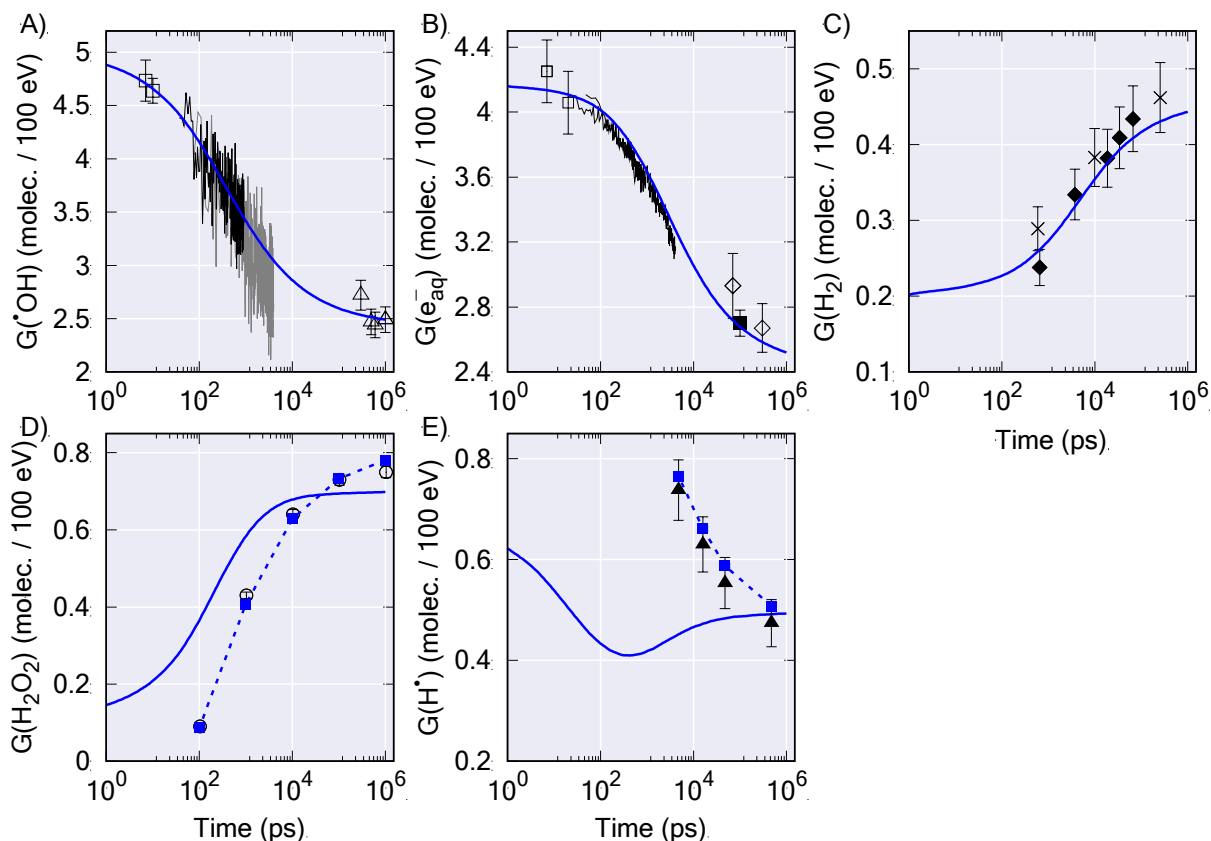


Figure 2 Time-dependent G values for fast electrons ($1 \text{ molec./100 eV} = 1.036 \times 10^{-7} \text{ mol J}^{-1}$). TOPAS-nBio/Geant4-DNA simulated data: (solid line) pure liquid water calculations; (blue squares connected with dashed lines) simulations of scavenger systems for H_2O_2 and H^* as shown in table 1. Error bars represent statistical uncertainties, one standard deviation. Measured data: black and grey solid lines (Ma et al 2015); \square (Wang et al 2018); Δ (Laverne 2000); \square (Bartels et al 2000); \diamond (Shiraishi et al 1988); \times and \blacklozenge (Pastina et al 1999); \circ (Hiroki et al 2002); \blacktriangle (Huerta Parajon et al 2008).

3 Results.

3.1 Time-dependent G values for fast electrons.

It was found that a distance of four water molecule's mean separation distances, 1.24 nm, for both $\text{RMS}^{\text{H}_2\text{O}^+}$ and $\text{RMS}^{\text{H}_2\text{O}^*}$ reproduced the measured time-dependent G values for $\cdot\text{OH}$ radicals. The G values using that value are shown in figure 2. In the top row of the figure, the calculated G value in pure liquid water for $\cdot\text{OH}$, e_{aq}^- and H_2 are displayed in individual panels, along with experimental data. The agreement for the three sets of data along all the time domains was within one standard deviation of experimental measurements. In the bottom row of figure 2, the G value for H_2O_2 and H^* is displayed in each panel. As depicted, the time-

dependent G values calculated in pure liquid water (solid line) did not reproduce the behavior of the experimental yields for H₂O₂ (empty circles) and H[•] (filled triangles). However, the simulations considering the scavengers used in the experiments (squares connected by dashed lines) agreed within one standard deviation of the experimental data.

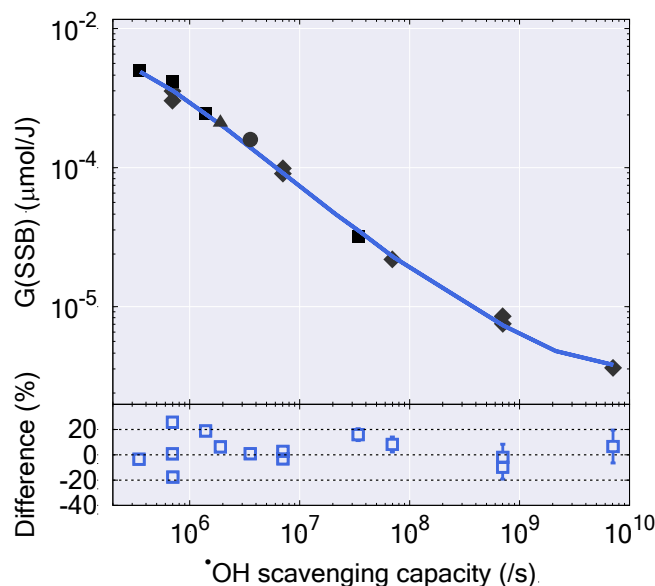


Figure 3 Total calculated SSB yields (direct plus indirect) as a function of \bullet OH scavenging capacity (solid lines). Measured data for pUC18 is from \blacksquare (Milligan et al 1993), \blacklozenge (Milligan and Ward 1994), and \bullet (Milligan et al 1996). Measured data for pUC19 \blacktriangle is from (Perry et al 2021). Percentage differences (\square) between calculated to measured data are shown in the bottom figure. The dotted lines are margins from experimental uncertainty. Error bars are displayed when bigger than the symbol, represent statistical uncertainties from Monte Carlo simulations, one standard deviation.

3.2 DNA damage in plasmid geometries.

In figure 3, calculated and measured SSB yields as a function of \bullet OH scavenging capacity are shown. The estimated efficiencies for \bullet OH and H[•] are 24% and 0.5%, respectively. These values are used in all the following results. As depicted, the calculated SSB yields reproduced the measured data from pUC18 irradiations along with the considered DMSO concentrations reasonably well. The yields included the G(SSB) produced by direct effects, which resulted in $1.77 \pm 0.01 \times 10^{-6} \mu\text{mol/J}$ for the geometrical DNA model used in this work. Figure 4 shows G(SSB) as a function of the DNA concentration. The slopes of linear regression fitting to both calculated and measured data agreed within $1\% \pm 0.8\%$. Finally, calculated DBS as a function of \bullet OH scavenging capacity reproduced the behavior of measured yields well as shown in figure 5.

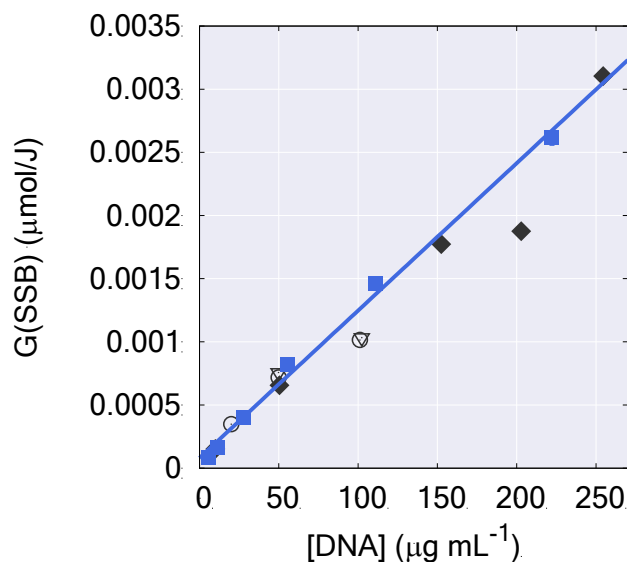


Figure 4 Calculated $G(\text{SSB})$ as a function of the DNA concentration (\blacksquare connected with solid line). Error bars, smaller than the symbols, represent statistical uncertainties, one standard deviation. Measured data is from (Milligan et al 1993): pUC18 (○); pEC (△); and SV40 (◆).

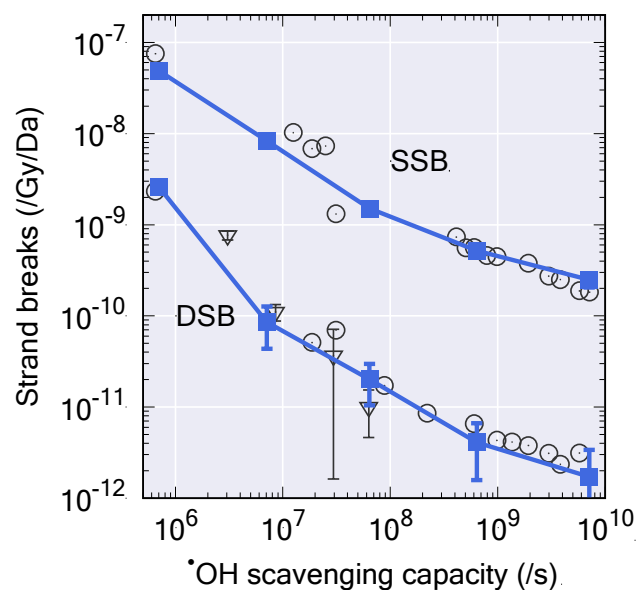


Figure 5 Calculated single and double-strand break yields as a function of hydroxyl radical scavenging capacity. Error bars represent statistical uncertainties, one standard deviation. Measured data: ○ pBR322 (Klimczak et al 1993), ▽ pBR322 (Tomita et al 1995).

4 Discussion.

In this work, TOPAS-nBio was applied to simulate water radiolysis and DNA damage under low-LET irradiation. The simulation of the reaction kinetics was performed with the IRT method,

1
2
3 providing a fast and reliable tool to assist in investigating the biological effect of the interaction
4 of ionizing radiation at the early stages.
5

6 Calculated G values at the picosecond stage agreed within experimental errors of
7 published direct measurements of $\cdot\text{OH}$ and e^-_{aq} performed in pure liquid water. The temporal
8 evolution of the G values simulated up to the microsecond time stage was also well reproduced
9 by TOPAS-nBio for $\cdot\text{OH}$, e^-_{aq} , and H_2 . To obtain such an agreement we adjusted the RMS of the
10 displacement of ionized and excited water molecules caused by charge migration. Oscillating
11 charge migration is expected to happen a few femtoseconds after an energy transfer event,
12 hence challenging its experimental observation given the short period of time (Kuleff *et al* 2016).
13 Thus, RMS values have been empirically adjusted in other Monte Carlo track-structure codes due
14 to the lack of corresponding measured data (Kreipl *et al* 2009, Cobut *et al* 1998, Tomita *et al*
15 1997, Uehara and Nikjoo 2006). The RMS obtained in this work (1.24 nm), shorter than Geant4-
16 DNA's default value (2 nm), increased the chance of contact reactions at the earliest times
17 producing lower yields of $\cdot\text{OH}$ radical. For $\cdot\text{OH}$ radicals at 7 ps, this modification represented a
18 reduction from 5.0 molecules per 100 eV (Ramos-Mendez *et al.*, 2020) to 4.7 molecules per 100
19 eV (the measure data show 4.7 ± 0.2 molecules per 100 eV (Wang *et al* 2018)). Geant4-DNA being
20 a radiation transport code is not currently capable of simulating molecular dynamics of water
21 molecules. Thus, effects like the binding of water molecules to biomolecules (DNA, proteins or
22 lipids) that in principle affect the RMS displacement (see e.g., Shweta and Sen 2018), cannot be
23 studied in detail at this point with our code. For e^-_{aq} , this parameter had a negligible effect as the
24 products of auto-ionization that followed a dissociation event were handled by the one-step
25 thermalization method (Shin *et al* 2019).
26
27
28
29

30 While it is a common practice, the comparison between time-dependent product yields
31 calculated in pure liquid water and measured data under the presence of scavengers deviated
32 from each other and should be avoided. In this work, two sets of data were selected to
33 demonstrate this point. The temporal evolution of H_2O_2 and H^\cdot reproduced the measured data
34 within experimental errors only when the yields were calculated in the presence of scavengers.
35 However, a more comprehensive evaluation of TOPAS-nBio under a wide range of scavengers,
36 scavenger concentrations, and radiation qualities was outside the scope of this work and it is the
37 subject of future work. A selection of radiobiologically relevant scavengers should precede that
38 task given the scope of TOPAS-nBio.
39
40

41 On the other hand, for DNA damage simulations an encouraging agreement was found
42 between calculated yields of SSB and DSB with measured data for low-LET radiation on a base-
43 pair level. A limitation of the applicability of IRT for smaller scales (e.g., including adenine,
44 thymine, cytosine, and guanine nucleobases or atomic components) could be expected. Bluett
45 and Green demonstrated (Bluett and Green 2006) that at such proximity, multiple reactive
46 centers in the sugar-base system might occur, so the reaction rate between a reaction pair is
47 affected by the presence of static neighboring species. The IRT method assumes that reactions
48 between pairs occur in isolation, thus, the IRT method may give inaccurate results. Nevertheless,
49 the use of observed reaction rates in this work provided a base-pair level resolution, which
50 resulted in a general agreement within experimental uncertainties.
51
52

53 The estimated SSB efficiencies from the Monte Carlo data included a highly detailed
54 plasmid DNA geometrical model. The estimated efficiency of 24% for SSB induction for $\cdot\text{OH}$ was
55 within previously reported values between 24% to 44% obtained with cylindrical non-
56
57
58
59
60

1
2
3 homogeneous kinetic model (Milligan *et al* 1993, Udovičić *et al* 1994, Klimczak *et al* 1993). In that
4 model, however, a homogenous cylindrical model representing a straight DNA segment was
5 considered, which differed from the more detailed supercoiling DNA representation facilitated
6 by TOPAS-nBio. For H^{*}, the efficiency of 0.5% provided the best agreement at higher scavenger
7 concentrations. This value was close to the 0.81% calculated by (Aydogan *et al* 2008). The
8 differences are subtle and could be attributed to the different Monte Carlo codes used by
9 these authors. In their model, the authors used a straight linear DNA segment of 38 bp, with
10 atomic resolution and multiple reactions sites on a base pair. However, our calculated efficiency
11 was 12% higher than that measured experimentally (Milligan *et al* 1993). This difference may be
12 due to the limited resolution of our model, justified by the use of the variable rate coefficient for
13 •OH + DNA, which disregards the individual reactions with nucleobases and other components.
14 The reaction of •OH with nucleobases is in general several times faster than the reaction of •OH
15 with deoxyribose (Buxton *et al* 1988). Thus, by including reactions with DNA bases, an increment
16 in the number of •OH reactions is expected, which might lead to a lower SSB efficiency. For that,
17 reaction rate constants obtained in a B-DNA structure instead of an aqueous solution of DNA are
18 needed. From the computational point of view, an effort of our group to find ways to extend the
19 IRT method to handle DNA bases was reported in (Tran *et al* 2021). On the other hand, our
20 estimation of the direct effect assumed an energy threshold for accumulated energy depositions
21 of at least 17.5 eV, which produced 28% fewer SSB compared to, e.g., the 5-37.5 eV linear ramp
22 threshold shown elsewhere (Zhu *et al* 2020b). A more suitable selection of the energy threshold
23 must consider the transport of low energy electrons below 15 eV (avoiding the one-step
24 thermalization model), which can induce DNA damage, as shown experimentally by (Alizadeh *et al*
25 2015). In that regard, an extended physics package which improves the detail in the pre-
26 chemical stage for handling Auger electrons and electron capture will be soon made available in
27 Geant4 (Shin *et al.*, 2021 under review). Experimentally, a dependence with the scavenging
28 capacity of the SSB induction efficiency was further observed (Önal *et al* 1988). Even though we
29 used a single constant value as a first approach, the assumptions made in this work were
30 sufficient to reproduce the behavior of scavenging dependence of DSB yields measured for
31 different plasmids.
32
33
34
35
36
37
38
39

40 5 Conclusions.

41
42 In this work, TOPAS-nBio was validated for simulating water radiolysis in liquid water and DNA
43 damage for plasmids at low LET irradiation. Satisfactory agreement within experimental
44 uncertainties was obtained, reconciling Monte Carlo calculations of water radiolysis from •OH
45 and e⁻_{aq} yields at the picosecond level. For pUC18 plasmids irradiated by ¹³⁷Cs γ-rays, calibration
46 via the SSB induction efficiency was consistent with published efficiency values, leading to
47 agreement with measure data within experimental uncertainties. TOPAS-nBio facilitated the
48 implementation of experimental conditions of DNA irradiations including DNA geometry, source
49 quality, prescribed dose, chemical parameters, and scavengers, exploiting the full potential of
50 Geant4-DNA. As a result, an accurate, fast, and user-friendly Monte Carlo framework is provided
51 by TOPAS-nBio/Geant4-DNA to evaluate DNA damage from first principles.
52
53
54
55
56
57
58
59
60

Acknowledgments

This work was supported by NIH/NCI R01 CA187003 (TOPAS-nBio). V.Š. and K.S. were supported by the Czech Science Foundation project no. 17-03403Y. N.D-K. is a doctoral student from Programa de Doctorado en Ciencias Física Aplicada, Benemérita Universidad Autónoma de Puebla and received fellowship 2019-000002-01NACF-05024 from CONACYT, México.

References.

- Alizadeh E, Orlando T M and Sanche L 2015 Biomolecular damage induced by ionizing radiation: The direct and indirect effects of low-energy electrons on DNA *Annu. Rev. Phys. Chem.* **66** 379–98
- Arce P, Bolst D, Bordage M, Brown J M C, Cirrone P, Cortés-Giraldo M A, Cutajar D, Cuttone G, Desorgher L, Dondero P, Dotti A, Faddegon B, Fedon C, Guatelli S, Incerti S, Ivanchenko V, Konstantinov D, Kyriakou I, Latyshev G, Le A, Mancini-Terracciano C, Maire M, Mantero A, Novak M, Omachi C, Pandola L, Perales A, Perrot Y, Petringa G, Quesada J M, Ramos-Méndez J, Romano F, Rosenfeld A B, Sarmiento L G, Sakata D, Sasaki T, Sechopoulos I, Simpson E C, Toshito T and Wright D H 2021 Report on G4-Med, a Geant4 benchmarking system for medical physics applications developed by the Geant4 Medical Simulation Benchmarking Group *Med. Phys.* **48** 19–56 Online: <https://onlinelibrary.wiley.com/doi/abs/10.1002/mp.14226>
- Aydogan B, Bolch W E, Swarts S G, Turner J E and Marshall D T 2008 Monte Carlo Simulations of Site-Specific Radical Attack to DNA Bases *Radiat. Res.* **169** 223–31
- Bartels D M, Cook A R, Mudaliar M and Jonah C D 2000 Spur decay of the solvated electron in picosecond radiolysis measured with time-correlated absorption spectroscopy *J. Phys. Chem. A* **104** 1686–91
- Bernal M A, Bordage M C, Brown J M C, Davidková M, Delage E, El Bitar Z, Enger S A, Francis Z, Guatelli S, Ivanchenko V N, Karamitros M, Kyriakou I, Maigne L, Meylan S, Murakami K, Okada S, Payno H, Perrot Y, Petrovic I, Pham Q T, Ristic-Fira A, Sasaki T, Štěpán V, Tran H N, Villagrasa C and Incerti S 2015 Track structure modeling in liquid water: A review of the Geant4-DNA very low energy extension of the Geant4 Monte Carlo simulation toolkit. *Phys. Med.* **31** 861–74 Online: <http://www.sciencedirect.com/science/article/pii/S1120179715010042>
- Bluett V M and Green N J B 2006 Competitive diffusion-influenced reaction of a reactive particle with two static sinks *J. Phys. Chem. A* **110** 4738–52
- Boscolo D, Krämer M, Durante M, Fuss M C and Scifoni E 2018 TRAX-CHEM: A pre-chemical and chemical stage extension of the particle track structure code TRAX in water targets *Chem. Phys. Lett.* **698** 11–8 Online: <https://doi.org/10.1016/j.cplett.2018.02.051>
- Bruce W R, Pearson M L and Freedhoff H S 1963 The Linear Energy Transfer Distributions Resulting from Primary and Scattered X-Rays and Gamma Rays with Primary HVL's from 1.25 mm Cu to 11 mm Pb *Radiat. Res.* **19** 606 Online: <https://www.jstor.org/stable/3571481?origin=crossref>
- Burigo L, Pshenichnov I, Mishustin I, Hilgers G and Bleicher M 2016 Distributions of deposited energy and ionization clusters around ion tracks studied with Geant4 toolkit *Phys. Med.*

- 1
2
3 *Biol.* **61** 3698–711 Online: <http://stacks.iop.org/0031-9155/61/i=10/a=3698?key=crossref.6d36b15fba7d535b14de38a5fc3a9b1e>
- 4
5 Buxton G V., Greenstock C L, Helman W P and Ross A B 1988 Critical Review of rate constants
6 for reactions of hydrated electrons, hydrogen atoms and hydroxyl radicals in Aqueous
7 Solution *J. Phys. Chem. Ref. Data* **17** 513–886
- 8
9 Clifford P, Green N J B, Oldfield M J, Pilling M J and Pimblott S M 1986 Stochastic Models of
10 Multi-species Kinetics in Radiation-induced Spurs *J. Chem. Soc., Faraday Trans. 1* **82** 2673–
11 89
- 12
13 Cobut V, Frongillo Y, Patau J P, Goulet T, Fraser M J and Jay-Gerin J P 1998 Monte Carlo
14 simulation of fast electron and proton tracks in liquid water - I. Physical and
15 physicochemical aspects *Radiat. Phys. Chem.* **51** 229–43
- 16
17 Despré V, Marciniak A, Lorient V, Galbraith M C E, Rouzée A, Vrakking M J J, Lépine F and Kuleff A
18 I 2015 Attosecond hole migration in benzene molecules surviving nuclear motion *J. Phys.*
19 *Chem. Lett.* **6** 426–31
- 20
21 Dingfelder M, Hantke D, Inokuti M and Paretzke H G 1999 Electron inelastic-scattering cross
22 sections in liquid water *Radiat. Phys. Chem.* **53** 1–18
- 23
24 Edel S, Terrissol M, Peudon A, Kümmerle E and Pomplun E 2006 Computer simulation of strand
25 break yields in plasmid pBR322: DNA damage following 125I decay *Radiat. Prot. Dosimetry*
26 **122** 136–40
- 27
28 Faddegon B, Ramos-Méndez J, Schuemann J, McNamara A, Shin J, Perl J and Paganetti H 2020
29 The TOPAS tool for particle simulation, a Monte Carlo simulation tool for physics, biology
30 and clinical research *Phys. Medica* **72** 114–21 Online:
31 <https://doi.org/10.1016/j.ejmp.2020.03.019>
- 32
33 Friedland W, Schmitt E, Kunderát P, Dingfelder M, Baiocco G, Barbieri S and Ottolenghi A 2017
34 Comprehensive track-structure based evaluation of DNA damage by light ions from
35 radiotherapy-relevant energies down to stopping *Sci. Rep.* **7** 45161 Online:
36 <http://www.nature.com/articles/srep45161>
- 37
38 Fulford J, Nikjoo H, Goodhead D T and O'Neill P 2001 Yields of SSB and DSB induced in DNA by
39 Al K ultrasoft X-rays and α -particles: comparison of experimental and simulated yields *Int.*
40 *J. Radiat. Biol.* **77** 1053–66 Online:
41 <http://informahealthcare.com/doi/abs/10.1080/09553000110069308>
- 42
43 Green N J B, Pilling M J and Clifford P 1990 Stochastic Modeling of Fast Kinetics in a Radiation
44 Track *Society* **94** 251–8 Online: <http://pubs.acs.org/doi/abs/10.1021/j100364a041>
- 45
46 Hiroki A, Pimblott S M and Laverne J A 2002 Hydrogen peroxide production in the radiolysis of
47 water with high radical scavenger concentrations *J. Phys. Chem. A* **106** 9352–8
- 48
49 Huang J, Schlick T and Vologodskii A 2001 Dynamics of site juxtaposition in supercoiled DNA
50 *Proc. Natl. Acad. Sci. U. S. A.* **98** 968–73
- 51
52 Huerta Parajón M 2010 *HYDROGEN ATOM FORMATION IN THE GAMMA AND HEAVY ION*
53 *RADIOLYSIS OF AQUEOUS SYSTEMS A thesis submitted to The University of Manchester for*
54 *the (The University of Manchester)*
- 55
56 Huerta Parajon M, Rajesh P, Mu T, Pimblott S M and LaVerne J A 2008 H atom yields in the
57 radiolysis of water *Radiat. Phys. Chem.* **77** 1203–7
- 58
59 Incerti S, Baldacchino G, Bernal M, Capra R, Champion C, Francis Z, GuÈye P, Mantero A,
60 Mascialino B, Moretto P, Nieminen P, Villagrasa C and Zacharatou C 2010a THE Geant4-

- 1
2
3 DNA project *Int. J. Model. Simulation, Sci. Comput.* **1** 157–78
- 4 Incerti S, Ivanchenko A, Karamitros M, Mantero A, Moretto P, Tran H N, Mascialino B,
5 Champion C, Ivanchenko V N, Bernal M a, Francis Z, Villagrasa C, Baldacchin G, Guèye P,
6 Capra R, Nieminen P and Zacharatou C 2010b Comparison of GEANT4 very low energy
7 cross section models with experimental data in water. *Med. Phys.* **37** 4692–708
- 8 Incerti S, Kyriakou I, Bernal M A, Bordage M C, Francis Z, Guatelli S, Ivanchenko V, Karamitros
9 M, Lampe N, Lee S B, Meylan S, Min C H, Shin W G, Nieminen P, Sakata D, Tang N,
10 Villagrasa C, Tran H N and Brown J M C 2018 Geant4-DNA example applications for track
11 structure simulations in liquid water: A report from the Geant4-DNA Project *Med. Phys.* **45**
12 e722–39 Online: <http://doi.wiley.com/10.1002/mp.13048>
- 13 Jones G D D and O'Neill P 1991 Kinetics of radiation-induced Strand break formation in single-
14 stranded pyrimidine polynucleotides in the presence and absence of oxygen; a time-
15 resolved light-scattering study *Int. J. Radiat. Biol.* **59** 1127–45
- 16 Karamitros M, Mantero A, Incerti S, Friedland W, Baldacchino G, Barberet P, Bernal M, Capra R,
17 Champion C, El Bitar Z, Francis Z, Gueye P, Ivanchenko A, Ivanchenko V, Kurashige H,
18 Mascialino B, Moretto P, Nieminen P, Santin G, Seznec H, Tran H N, Villagrasa C and
19 Zacharatou C 2011 Modeling Radiation Chemistry in the Geant4 Toolkit *Prog. Nucl. Sci.*
20 *Technol.* **2** 503–8 Online: <http://www.aesj.or.jp/publication/pnst002/data/503-508.pdf>
- 21 Karamitros M 2012 Extension de l'outil Monte Carlo généraliste Geant4 pour la simulation de la
22 radiolyse de l'eau dans le cadre du projet Geant4-DNA [Doctoral dissertation, L'Université
23 Bordeaux 1] page 164: <http://www.theses.fr/2012BOR14629>.
- 24 Klimczak U, Ludwig D C, Mark F, Rettberg P and Schulte-Frohlinde D 1993 Irradiation of plasmid
25 and phage DNA in water-alcohol mixtures: Strand breaks and lethal damage as a function
26 of scavenger concentration *Int. J. Radiat. Biol.* **64** 497–510
- 27 Kreipl M S, Friedland W and Paretzke H G 2009 Time- and space-resolved Monte Carlo study of
28 water radiolysis for photon, electron and ion irradiation *Radiat. Environ. Biophys.* **48** 11–20
29 Online: <http://link.springer.com/10.1007/s00411-008-0194-8>
- 30 Kuleff A I, Kryzhevoi N V., Pernpointner M and Cederbaum L S 2016 Core Ionization Initiates
31 Subfemtosecond Charge Migration in the Valence Shell of Molecules *Phys. Rev. Lett.* **117**
32 1–5
- 33 Kumar A, Becker D, Adhikary A and Sevilla M D 2019 Reaction of electrons with dna: Radiation
34 damage to radiosensitization *Int. J. Mol. Sci.* **20**
- 35 Kümmerle E A and Pomplun E 2005 A computer-generated supercoiled model of the pUC19
36 plasmid *Eur. Biophys. J.* **34** 13–8 Online: <http://link.springer.com/10.1007/s00249-004-0431-2>
- 37 Lampe N, Karamitros M, Breton V, Brown J M C, Kyriakou I, Sakata D, Sarramia D and Incerti S
38 2018a Mechanistic DNA damage simulations in Geant4-DNA part 1: A parameter study in a
39 simplified geometry *Phys. Medica* **48** 135–45 Online:
40 <https://doi.org/10.1016/j.ejmp.2018.02.011>
- 41 Lampe N, Karamitros M, Breton V, Brown J M C, Sakata D, Sarramia D and Incerti S 2018b
42 Mechanistic DNA damage simulations in Geant4-DNA Part 2: Electron and proton damage
43 in a bacterial cell *Phys. Medica* **48** 146–55 Online:
44 <https://doi.org/10.1016/j.ejmp.2017.12.008>
- 45 Laverne J A 2000 OH Radicals and Oxidizing Products in the Gamma Radiolysis of Water *Source*
46
47
48
49
50
51
52
53
54
55
56
57
58
59
60

- 1
2
3 *Radiat. Res. Radiat. Res. Gamma Radiolysis Water. Radiat. Res* 53–196 Online:
4 <http://www.jstor.org/stable/3580071>
5
6 Ma J, Laverne J A and Mostafavi M 2015 Scavenging the Water Cation in Concentrated Acidic
7 Solutions *J. Phys. Chem. A* **119** 10629–36
8
9 Meylan S, Incerti S, Karamitros M, Tang N, Bueno M, Clairand I and Villagrasa C 2017 Simulation
10 of early DNA damage after the irradiation of a fibroblast cell nucleus using Geant4-DNA *Sci.*
11 *Rep.* **7** 1–15
12
13 Meylan S, Vimont U, Incerti S, Clairand I and Villagrasa C 2015 Geant4-DNA simulations using
14 complex DNA geometries generated by the DnaFabric tool *Comput. Phys. Commun.*
15
16 Milligan J R, Aguilera J A and Ward J F 1993 *Variation of Single-Strand Break Yield with*
17 *Scavenger Concentration for Plasmid DNA Irradiated in Aqueous Solution* vol 133 Online:
18 <http://www.jstor.org/stable/3578350?origin=crossref>
19
20 Milligan J R and Ward J F 1994 Yield of single-strand breaks due to attack on DNA by Scavenger-
21 derived radicals *Radiat. Res.* **137** 295–9
22
23 Milligan J R, Wu C C L, Ng J Y Y, Aguilera J A and Ward J F 1996 Characterization of the reaction
24 rate coefficient of DNA with the hydroxyl radical *Radiat. Res.* **146** 510–3 Online:
25 <http://www.jstor.org/stable/3579551>
26
27 Moiseenko V V., Hamm R N, Waker A J and Prestwich W V. 1998 The cellular environment in
28 computer simulations of radiation-induced damage to dna *Radiat. Environ. Biophys.* **37**
29 167–72
30
31 Nelder J A and Mead R 1965 A Simplex Method for Function Minimization *Comput. J.* **7** 308–13
32 Online: <https://academic.oup.com/comjnl/article-lookup/doi/10.1093/comjnl/8.1.27>
33
34 Nikjoo H, Emfietzoglou D, Liamsuwan T, Taleei R, Liljequist D and Uehara S 2016 Radiation track,
35 DNA damage and response—a review *Reports Prog. Phys.* **79** 116601 Online:
36 [http://stacks.iop.org/0034-](http://stacks.iop.org/0034-4885/79/i=11/a=116601?key=crossref.97c4492091d158513ac8241fafa018bf)
37 [4885/79/i=11/a=116601?key=crossref.97c4492091d158513ac8241fafa018bf](http://stacks.iop.org/0034-4885/79/i=11/a=116601?key=crossref.97c4492091d158513ac8241fafa018bf)
38
39 Ogura H and Hamill W H 1973 Positive hole migration in pulse-irradiated water and heavy water
40 *J. Phys. Chem.* **77** 2952–4
41
42 El Omar A K, Schmidhammer U, Jeunesse P, Larbre J P, Lin M, Muroya Y, Katsumura Y, Pernot P
43 and Mostafavi M 2011 Time-dependent radiolytic yield of OH• radical studied by
44 picosecond pulse radiolysis *J. Phys. Chem. A* **115** 12212–6 Online:
45 <http://pubs.acs.org/doi/pdf/10.1021/jp208075v>
46
47 Önal A M, Lemaire D G E, Bothe E and Schulte-Frohlinde D 1988 γ radiolysis of poly(a) in
48 aqueous solution: Efficiency of Strand break formation by primary water radicals *Int. J.*
49 *Radiat. Biol.* **53** 787–96
50
51 Pastina B and LaVerne J A 1999 Hydrogen Peroxide Production in the Radiolysis of Water with
52 Heavy Ions *J. Phys. Chem. A* **103** 1592–7 Online:
53 <http://pubs.acs.org/doi/abs/10.1021/jp984433o>
54
55 Pastina B, Laverne J A and Pimblott S M 1999 Dependence of Molecular Hydrogen Formation in
56 Water on Scavengers of the Precursor to the Hydrated Electron *J. Phys. Chem. A* **103** 5841–
57 6 Online: <https://pubs.acs.org/doi/pdf/10.1021/jp991222q>
58
59 Perkins S J 1986 Protein volumes and hydration effects. The calculations of partial specific
60 volumes, neutron scattering matchpoints and 280-nm absorption coefficients for proteins
and glycoproteins from amino acid sequences *Eur. J. Biochem.* **157** 169–80 Online:

- 1
2
3 <http://www.ncbi.nlm.nih.gov/pubmed/3709531>
- 4 Perl J, Shin J, Schümann J, Faddegon B and Paganetti H 2012 TOPAS: An innovative proton
5 Monte Carlo platform for research and clinical applications *Med. Phys.* **39** 6818–37 Online:
6 <http://doi.wiley.com/10.1118/1.4758060>
- 7
8 Perry C C, Ramos-Méndez J and Milligan J R 2021 Boronated Condensed DNA as a
9 Heterochromatic Radiation Target Model *Biomacromolecules* *acs.biomac.1c00106* Online:
10 <https://pubs.acs.org/doi/10.1021/acs.biomac.1c00106>
- 11
12 Perry C C, Ramos-Méndez J and Milligan J R 2020 DNA condensation with a boron-containing
13 cationic peptide for modeling boron neutron capture therapy *Radiat. Phys. Chem.* **166**
14 108521 Online: <https://linkinghub.elsevier.com/retrieve/pii/S0969806X19311417>
- 15
16 Pimblott S M 1992 Investigation of various factors influencing the effect of scavengers on the
17 radiation chemistry following the high-energy electron radiolysis of water *J. Phys. Chem.*
18 **96** 4485–91 Online: <https://pubs.acs.org/doi/pdf/10.1021/j100190a066>
- 19
20 Pimblott S M and LaVerne J A 1997 Stochastic Simulation of the Electron Radiolysis of Water
21 and Aqueous Solutions *J. Phys. Chem. A* **101** 5828–38 Online:
22 <http://pubs.acs.org/doi/abs/10.1021/jp970637d>
- 23
24 Pimblott S M, LaVerne J A, Bartels D M and Jonah C D 1996 Reconciliation of Transient
25 Absorption and Chemically Scavenged Yields of the Hydrated Electron in Radiolysis *J. Phys.*
26 *Chem.* **100** 9412–5 Online: <https://pubs.acs.org/doi/pdf/10.1021/jp960816f>
- 27
28 Pimblott S M, Pilling M J and Green N J B 1991 Stochastic models of spur kinetics in water *Int. J.*
29 *Radiat. Appl. Instrumentation. Part* **37** 377–88
- 30
31 Plante I and Devroye L 2017 Considerations for the independent reaction times and step-by-
32 step methods for radiation chemistry simulations *Radiat. Phys. Chem.* **139** 157–72 Online:
33 <http://dx.doi.org/10.1016/j.radphyschem.2017.03.021>
- 34
35 Ramos-Méndez J, Domínguez-Kondo N, Schuemann J, McNamara A, Moreno-Barbosa E and
36 Faddegon B 2020 LET-Dependent Intertrack Yields in Proton Irradiation at Ultra-High Dose
37 Rates Relevant for FLASH Therapy *Radiat. Res.* **194** 5–7 Online:
38 [https://bioone.org/journals/radiation-research/volume-194/issue-4/RADE-20-
39 00084.1/LET-Dependent-Intertrack-Yields-in-Proton-Irradiation-at-Ultra-
40 High/10.1667/RADE-20-00084.1.full](https://bioone.org/journals/radiation-research/volume-194/issue-4/RADE-20-00084.1/LET-Dependent-Intertrack-Yields-in-Proton-Irradiation-at-Ultra-High/10.1667/RADE-20-00084.1.full)
- 41
42 Ramos-Méndez J, Perl J, Schuemann J, McNamara A, Paganetti H and Faddegon B 2018 Monte
43 Carlo simulation of chemistry following radiolysis with TOPAS-nBio *Phys. Med. Biol.* **63**
44 105014 Online: <http://iopscience.iop.org/article/10.1088/1361-6560/aac04c>
- 45
46 Ramos-Méndez J, Shin W, Karamitros M, Domínguez-Kondo J, Tran N H, Incerti S, Villagrasa C,
47 Perrot Y, Štěpán V, Okada S, Moreno-Barbosa E and Faddegon B 2020 Independent
48 reaction times method in Geant4-DNA: Implementation and performance *Med. Phys.* **47**
49 5919–30 Online: <https://onlinelibrary.wiley.com/doi/10.1002/mp.14490>
- 50
51 Ritchie R H, Hamm R N, Turner J E and Bolch W E 1994 Interactions of Low-Energy Electrons
52 with Condensed Matter: Relevance for Track Structure *Computational Approaches in*
53 *Molecular Radiation Biology* (Boston, MA: Springer US) pp 33–47 Online:
54 http://link.springer.com/10.1007/978-1-4757-9788-6_4
- 55
56 Sakata D, Lampe N, Karamitros M, Kyriakou I, Belov O, Bernal M A, Bolst D, Bordage M-C C,
57 Breton V, Brown J M C, Francis Z, Ivanchenko V, Meylan S, Murakami K, Okada S, Petrovic I,
58 Ristic-Fira A, Santin G, Sarramia D, Sasaki T, Shin W-G G, Tang N, Tran H N, Villagrasa C,
59
60

- 1
2
3 Emfietzoglou D, Nieminen P, Guatelli S and Incerti S 2019 Evaluation of early radiation DNA
4 damage in a fractal cell nucleus model using Geant4-DNA *Phys. Medica* **62** 152–7 Online:
5 <https://doi.org/10.1016/j.ejmp.2019.04.010>
6
- 7 Sanguanmith S, Meesungnoen J and Jay-Gerin J P 2013 Time-dependent yield of OH radicals in
8 the low linear energy transfer radiolysis of water between 25 and 350 °C *Chem. Phys. Lett.*
9 **588** 82–6 Online: <http://dx.doi.org/10.1016/j.cplett.2013.09.057>
10
- 11 Schuemann J, McNamara A L, Ramos-Méndez J, Perl J, Held K D, Paganetti H, Incerti S and
12 Faddegon B 2018 TOPAS-nBio: An Extension to the TOPAS Simulation Toolkit for Cellular
13 and Sub-cellular Radiobiology *Radiat. Res.* **191** 125 Online:
14 <http://www.rrjournal.org/doi/pdf/10.1667/RR15226.1>
15
- 16 Shin W-G, Ramos-Mendez J, Faddegon B, Tran H N, Villagrasa C, Perrot Y, Okada S, Karamitros
17 M, Emfietzoglou D, Kyriakou I, Bordage M C, Sakata D, Guatelli S, Choi H J, Min C H, Lee S B
18 and Incerti S 2019 Evaluation of the influence of physical and chemical parameters on
19 water radiolysis simulations under MeV electron irradiation using Geant4-DNA *J. Appl.*
20 *Phys.* **126** 114301 Online: <http://aip.scitation.org/doi/10.1063/1.5107511>
21
- 22 Shin W G, Bordage M C, Emfietzoglou D, Kyriakou I, Sakata D, Min C H, Lee S B, Guatelli S and
23 Incerti S 2018 Development of a new Geant4-DNA electron elastic scattering model for
24 liquid-phase water using the ELSEPA code *J. Appl. Phys.* **124** Online:
25 <http://dx.doi.org/10.1063/1.5047751>
26
- 27 Shiraishi H, Katsumura Y, Hiroishi D, Ishigure K and Washio M 1988 Pulse-radiolysis study on the
28 yield of hydrated electron at elevated temperatures *J. Phys. Chem.* **92** 3011–7 Online:
29 <http://pubs.acs.org/doi/abs/10.1021/j100321a061>
30
- 31 Shweta H and Sen S 2018 Dynamics of water and ions around DNA: What is so special about
32 them? *J Biosci* **43** 499–518
33
- 34 Štěpán V and Davídková M 2014 RADAMOL tool: Role of radiation quality and charge transfer in
35 damage distribution along DNA oligomer Guest editors: Andrey V. Solov'yov, Nigel Mason,
36 Paulo Limão-Vieira, Malgorzata Smialek-Telega *Eur. Phys. J. D* **68**
37
- 38 Sultana A, Meesungnoen J and Jay-Gerin J P 2020 Yields of primary species in the low-linear
39 energy transfer radiolysis of water in the temperature range of 25-700 °c *Phys. Chem.*
40 *Chem. Phys.* **22** 7430–9
41
- 42 Tachiya M 1983 Theory of diffusion-controlled reactions: Formulation of the bulk reaction rate
43 in terms of the pair probability *Radiat. Phys. Chem.* **21** 167–75 Online:
44 <https://linkinghub.elsevier.com/retrieve/pii/0146572483901437>
45
- 46 Tomita H, Kai M, Kusama T and Aoki Y 1995 Strand Break Formation in Plasmid DNA Irradiated
47 in Aqueous Solution: Effect of Medium Temperature and Hydroxyl Radical Scavenger
48 Concentration. *J. Radiat. Res.* **36** 46–55 Online: [https://academic.oup.com/jrr/article-
49 lookup/doi/10.1269/jrr.36.46](https://academic.oup.com/jrr/article-lookup/doi/10.1269/jrr.36.46)
50
- 51 Tomita H, Kai M, Kusama T and Ito A 1998 Monte Carlo simulation of DNA strand-break
52 induction in supercoiled plasmid pBR322 DNA from indirect effects *Radiat. Environ.*
53 *Biophys.* **36** 235–41 Online: <http://link.springer.com/10.1007/s004110050077>
54
- 55 Tomita H, Kai M, Kusama T and Ito A 1997 Monte Carlo simulation of physicochemical
56 processes of liquid water radiolysis *Radiat. Environ. Biophys.* **36** 105–16 Online:
57 <http://link.springer.com/10.1007/s004110050061>
58
- 59 Tran H N, Ramos-Méndez J, Shin W, Perrot Y, Faddegon B, Okada S, Karamitros M, Davídková
60

- 1
2
3 M, Štěpán V, Incerti S and Villagrasa C 2021 Assessment of DNA damage with an adapted
4 independent reaction time approach implemented in Geant4-DNA for the simulation of
5 diffusion-controlled reactions between radio-induced reactive species and a chromatin
6 fiber *Med. Phys.* **48** 890–901 Online:
7 <https://onlinelibrary.wiley.com/doi/10.1002/mp.14612>
- 8
9 Udovičić L, Mark F, Bothe E and Udovicic L 1994 Yields of Single-Strand Breaks in Double-
10 Stranded Calf Thymus DNA Irradiated in Aqueous Solution in the Presence of Oxygen and
11 Scavengers *Radiat. Res.* **140** 166 Online:
12 <https://www.jstor.org/stable/3578899?origin=crossref>
- 13
14 Uehara S and Nikjoo H 2006 Monte Carlo simulation of water radiolysis for low-energy charged
15 particles. *J. Radiat. Res.* **47** 69–81
- 16
17 Vologodskii A V. and Cozzarelli N R 1994 Conformational and thermodynamic properties of
18 supercoiled DNA *Annu. Rev. Biophys. Biomol. Struct.* **23** 609
- 19
20 Wang F, Schmidhammer U, Larbre J P, Zong Z, Marignier J L and Mostafavi M 2018 Time-
21 dependent yield of the hydrated electron and the hydroxyl radical in D2O: A picosecond
22 pulse radiolysis study *Phys. Chem. Chem. Phys.* **20** 15671–9
- 23
24 Wardman P 2020 Radiotherapy Using High-Intensity Pulsed Radiation Beams (FLASH): A
25 Radiation-Chemical Perspective *Radiat. Res.* **194** Online:
26 [https://bioone.org/journals/radiation-research/volume-194/issue-6/RADE-19-](https://bioone.org/journals/radiation-research/volume-194/issue-6/RADE-19-00016/Radiotherapy-Using-High-Intensity-Pulsed-Radiation-Beams-FLASH--A/10.1667/RADE-19-00016.full)
27 [00016/Radiotherapy-Using-High-Intensity-Pulsed-Radiation-Beams-FLASH--](https://bioone.org/journals/radiation-research/volume-194/issue-6/RADE-19-00016/Radiotherapy-Using-High-Intensity-Pulsed-Radiation-Beams-FLASH--A/10.1667/RADE-19-00016.full)
28 [A/10.1667/RADE-19-00016.full](https://bioone.org/journals/radiation-research/volume-194/issue-6/RADE-19-00016/Radiotherapy-Using-High-Intensity-Pulsed-Radiation-Beams-FLASH--A/10.1667/RADE-19-00016.full)
- 29
30 Yanisch-Perron C, Vieira J and Messing J 1985 Improved M13 phage cloning vectors and host
31 strains: nucleotide sequences of the M13mpl8 and pUC19 vectors *Gene* **33** 103–19 Online:
32 <https://linkinghub.elsevier.com/retrieve/pii/0378111985901209>
- 33
34 Zhu H, McNamara A L, McMahon S J, Ramos-Mendez J, Henthorn N T, Faddegon B, Held K D,
35 Perl J, Li J, Paganetti H and Schuemann J 2020a Cellular Response to Proton Irradiation: A
36 Simulation Study with TOPAS-nBio *Radiat. Res.* **194** 9 Online:
37 <http://www.rrjournal.org/doi/10.1667/RR15531.1>
- 38
39 Zhu H, McNamara A L, Ramos-Mendez J, McMahon S J, Henthorn N T, Faddegon B, Held K D,
40 Perl J, Li J, Paganetti H and Schuemann J 2020b A parameter sensitivity study for
41 simulating DNA damage after proton irradiation using TOPAS-nBio *Phys. Med. Biol.* **65**
42 085015 Online: <https://iopscience.iop.org/article/10.1088/1361-6560/ab7a6b>
43
44
45
46
47
48
49
50
51
52
53
54
55
56
57
58
59
60